AJNR

Imaging Features of Craniofacial Giant Cell Granulomas: A Large Retrospective Analysis from a Tertiary Care Center

R. Chanda, S.S. Regi, M. Kandagaddala, A. Irodi, M. Thomas and M. John

AJNR Am J Neuroradiol 2022, 43 (8) 1190-1195
doi: https://doi.org/10.3174/ajnr.A7568
http://www.ajnr.org/content/43/8/1190

Imaging Features of Craniofacial Giant Cell Granulomas: A Large Retrospective Analysis from a Tertiary Care Center

R. Chanda, S.S. Regi, M. Kandagaddala, A. Irodi, M. Thomas, and M. John

ABSTRACT

BACKGROUND AND PURPOSE: Craniofacial giant cell granulomas are rare lesions with varied appearances on imaging. We aimed to describe the imaging features of giant cell granulomas of the craniofacial bones.

MATERIALS AND METHODS: A retrospective analysis of the clinical features and imaging findings of 20 histopathology-proved cases of craniofacial giant cell granulomas, dating from 2006 to 2022, was performed.

RESULTS: Of the 20 cases, 10 each were seen in men and women. The epicenter of the lesions varied in location: in the maxilla in 8 patients, in the mandible in 5, in the temporal bone in 3, in the sphenoid/clivus in 3, and in the orbit in 1 patient. On the radiographs, the lesions appeared well-circumscribed, expansile, and lytic. On CT, the lesions were predominantly multiloculated, with thin septa, a soft-tissue component, and with expansion and remodeling of the underlying bone. On MR imaging, the solid component of the lesions was isointense on T1WI and hypointense on T2WI, with heterogeneous enhancement of the solid component and rim enhancement of the locules. Fluid-fluid levels were present in 3 patients.

CONCLUSIONS: Giant cell granulomas commonly present as locally aggressive, expansile, multiloculated lytic lesions, with solid as well as cystic areas. The solid component is typically hypointense on T2WI. Certain key imaging features of giant cell granulomas can aid the radiologist in narrowing the differential diagnosis.

ABBREVIATIONS: ABC = aneurysmal bone cyst; GCG = giant cell granuloma; GCRG = giant cell reparative granuloma; GCT = giant cell tumor

The term central giant cell reparative granuloma (GCRC) was first used by Jaffe,[1] in 1953, to describe a lesion that developed in response to intraosseous hemorrhage. There has been much debate about the presence of the reparative component in the pathogenesis of these granulomas;[2] hence, the term giant cell granuloma (GCG) is preferred compared with GCRG. Endosteal GCGs are classified as central, while those arising in the soft tissue are peripheral GCGs. The World Health Organization 2017 classification (updated version) of head and neck tumors classifies GCGs under giant cell lesions along with cherubism, aneurysmal bone cyst (ABC), and simple bone cyst.[3,4]

The craniofacial bones are the usual sites of involvement, followed by small bones of the hands and feet.[5] GCGs of the head and neck region are known to show a female predilection, with some lesions showing accelerated growth during pregnancy, suggesting a possible hormone-dependent nature of these lesions.[6]

Varied imaging appearances of GCGs pose a diagnostic challenge in differentiating them from other bone lesions such as ABCs, brown tumors, fibrous dysplasia, various odontogenic and nonodontogenic cysts, maxillofacial malignancies, and giant cell tumors (GCTs).

On histopathology, GCGs consist of spindled fibroblasts, collagenous stroma, areas of hemorrhage, and numerous multinucleated, osteoclast-type giant cells arranged in small clusters around areas of hemorrhage, usually containing ≤12 nuclei. Secondary changes with hemosiderin deposits, aggregates of foamy macrophages, cystic changes, and reactive bone formation may be seen in GCGs, simulating an ABC.

Solid ABCs have slender and spindle-shaped mononuclear cells and clustering of giant cells resembling GCGs. However, woven bone trabeculae are prominent in ABCs, while hemorrhagic foci are less conspicuous.[7,8] A *USP6* gene rearrangement is seen in ABCs.[9]

GCGs are indistinguishable from brown tumors of hyperparathyroidism on imaging as well as histopathology, with brown tumors usually containing more fibrous septa that

Received March 27, 2022; accepted after revision May 24.

From the Departments of Radiodiagnosis (R.C., S.S.R., M.K., A.I.), Pathology (M.T.), and Otorhinolaryngology (M.J.), Christian Medical College, Vellore, India.

Dr. R. Chanda is first author.

Please address correspondence to Madhavi Kandagaddala, DNB, Department of Radiodiagnosis, Christian Medical College, Vellore, Tamil Nadu, India 632004; e-mail: madhoo116@gmail.com

http://dx.doi.org/10.3174/ajnr.A7568

Table 1: Key histopathologic features of common differentials of GCGs

	GCG	GCT	ABC	Brown Tumor
Epithelioid stroma	Spindled stroma, oval-to-elongated nuclei	Plump epithelioid with oval nuclei	Spindled stroma, oval-to-elongated nuclei	Spindled stroma, oval-to-elongated nuclei with fibrous stroma dividing it into lobules
Giant cells	12 Nuclei in clusters around hemorrhagic foci	>12 Uniformly distributed nuclei	Smaller giant cells, in clusters, woven bone present, less hemorrhage	Few giant cells
Immunohistochemistry (p63 positivity)	Yes	Yes	No	No
Gene mutation				
H3f3a mutation	No	Yes	No	No
USP6 rearrangement	No	No	Yes	No

subcompartmentalize these lesions into multiple lobules.[3,5] On histology, GCGs are also indistinguishable from cherubism.

The mononuclear cells in GCGs are spindle-shaped and not oval or round as in GCT of the bones, with fewer mitotic figures.[7,8] GCTs histologically have numerous large, osteoclast-type giant cells, evenly distributed throughout the tumor with >12 nuclei. The mononuclear cells are arranged in a syncytial pattern in GCTs. On immunohistochemistry, both GCTs and GCGs can show an expression of p63 in mononuclear cells. Mutations in the *H3f3a* gene are seen in GCTs, but not in GCGs.[10-12]

A summary of the key histopathologic features of GCGs, GCTs, ABCs, and brown tumors is provided in Table 1.

It is important to differentiate GCTs and GCGs because the former is associated with a higher recurrence rate, malignant transformation, and metastatic potential compared with the latter.[13]

In this study, we report our experiences and observations from a large case series to highlight the key imaging features of GCGs that could aid in narrowing the differential diagnosis.

MATERIALS AND METHODS

In this institutional review board–approved study, all cases of craniofacial GCGs diagnosed on imaging at our tertiary care center and confirmed by histopathology during 15 years, between 2006 to 2022, were included in this study. A retrospective analysis of their imaging findings was conducted.

The study began with a PACS search using the keywords "GCRG," "GCG," and "giant" in CT and MR imaging modalities. This yielded a list of 33 craniofacial lesions in which GCG was provided as the radiologic/differential diagnosis. Of these cases, 24 patients underwent biopsy and 20 cases were confirmed as GCGs, which were then included in this study. Of the remaining 9 cases, 8 patients did not undergo biopsy and 1 lesion was diagnosed as pyogenic granuloma on histopathology. Thus, these cases were excluded from the study.

Of the 20 patients included in the study, local radiographs were available for 9 patients, of which 8 were orthopantomograms and 1 was a paranasal sinus radiograph. Both CT and MR imaging were performed in 8 patients, and only CT was performed in 12 patients. CT scans were performed using Somatom Emotion 16-section (Siemens) or Discovery 750 HD 128-section (GE Healthcare) scanners with a section thickness of 2 mm, FOV of 230 × 230, and a bolus injection of iohexol in soft-tissue and bone algorithms.

The MR imaging studies were performed on either 1.5T (Avanto; Siemens) or 3T (Achieva; Philips Healthcare) scanners with similar imaging protocols and acquisition parameters: Achieva, 3T T1-weighted spin-echo sequence (TE/TR = 20/630 ms; echo-train length = 6; flip angle = 90°; section thickness = 5 mm; section gap = 0.5); T2-weighted spin-echo sequence (TE/TR = 90/3500 ms; echo-train length = 13; flip angle = 90°; section thickness = 5 mm; section gap = 0.5); and STIR T2-weighted spin-echo sequence (TE/TR = 60/4000 ms; echo-train length = 11; flip angle = 160°); Avanto, 1.5T T1-weighted spin-echo sequence (TE/TR = 17/460 ms; echo-train length = 3; flip angle = 90°; number of averages = 2; section gap = 0.5); T2-weighted spin-echo sequence (TE/TR = 80/3000 ms; echo-train length = 13; flip angle = 90°; section gap = 0.5); and STIR T2-weighted spin-echo sequence (TE/TR = 70/3000 ms; echo-train length = 11; flip angle = 160°). Postcontrast T1-weighted sequences were obtained after a bolus injection of 0.1 mmol/kg of gadoteric acid. SWI and DWI (b-value = 800) with ADC mapping were available for 4 patients.

The 20 confirmed lesions were assessed for location, size, number, extension, margins, matrix, septations, and loculations on all imaging modalities. Additionally, on CT, bony remodeling, tooth resorption, matrix mineralization, enhancement, and extraosseous extension were assessed. On MR imaging, intralesional signal characteristics were assessed on T1WI, T2WI, STIR, SWI, DWI, and postcontrast sequences. Intracranial extension was also assessed on both CT and MRI. Lesions with radiologic features, such as tooth resorption, the presence of extraosseous soft-tissue components, and loss of plane with surrounding structures were classified as aggressive. On the other hand, lesions that were confined to the bone and showed scalloping, rather than erosion of the bone, displacing rather than infiltrating the surrounding structures, were classified as nonaggressive types.

The imaging findings were reviewed by 2 radiologists (R.C. and S.S.R.) with 5 and 6 years of experience, respectively.

RESULTS

Patient Demographics

The 20 patients comprised 10 male and 10 female cases. The mean age of the patients was 28 years (range, 7–65 years); there were 8 pediatric and 12 adult patients. A sex-based distribution of the location of GCGs is provided in Table 2.

Table 2: Sex-wise distribution of craniofacial GCGs

	Male	Female	Total
Orbit	1	0	1
Mandible	3	2	5
Maxilla	3	5	8
Temporal	1	2	3
Sphenoid/clivus	2	1	3

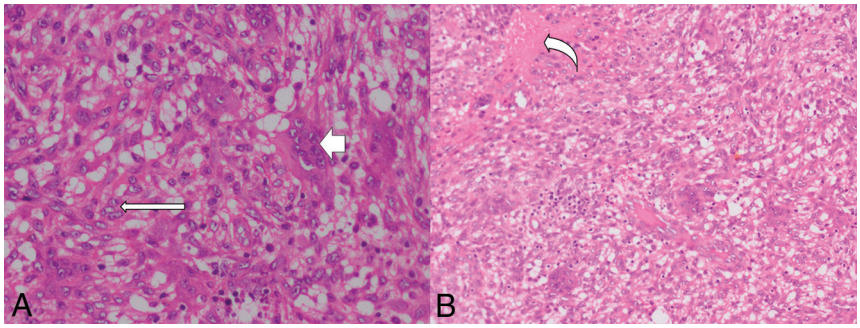

FIG 1. *A*, H&E, original magnification ×200. Cellular lesion composed of sheets of oval- to spindle-shaped cells admixed with many multinucleated giant cells (*short arrow*), the nuclei of which resemble stromal cells (*long arrow*). Mitotic activity is inconspicuous. *B*, H&E original magnification ×100. Hemorrhagic foci (*curved arrow*) and mild lymphocytic infiltrates in the surrounding stroma.

Clinical Presentation

The most common presenting symptom was painless, progressive swelling ($n = 13$). Four patients presented with recurrent episodes of bleeding ($n = 2$ with oral bleed, $n = 1$ with epistaxis, $n = 1$ ear bleed).

Region-specific symptoms, such as otorrhea, ear pain for temporal lesions, diplopia and visual disturbance in lesions involving the orbit, nasal obstruction, and discharge in lesions with nasal extension were also seen. GCG was incidentally identified in 1 patient who underwent a CT of the neck for a soft-tissue lesion in the right parapharyngeal space. Most patients ($n = 16$) presented within 1 year of onset of symptoms. There was no reported history of malignancy, hyperparathyroidism, radiation therapy, or regional trauma in any patient. Among the female patients, there was no reported history of occurrence of a new lesion or change in the size of an existing lesion during pregnancy.

Histopathology Features

Histopathologic diagnosis of GCG was confirmed by the presence of an ill-circumscribed cellular lesion, composed of sheets of oval- to spindle-shaped cells with vesicular nuclei, visible nucleoli, and moderate amounts of eosinophilic cytoplasm, with adjacent areas of stromal fibrosis, hemorrhage, and congested blood vessels (Fig 1). Interspersed with this stroma were many multinucleated giant cells, the nuclei of which resembled the stromal cells. Mitotic activity was inconspicuous. Three lesions with multiple fluid-fluid levels on MR imaging showed features of GCG with secondary ABC on histopathological examination.

Tumor Location and Extension

All 20 lesions in this study were central GCGs, originating in the craniofacial and/or skull base bones; we did not encounter any soft-tissue/peripheral GCGs. The epicenter of 8 lesions was in the maxilla, 5 involved the mandible, 3 were in the temporal bone, another 3 were in the sphenoid sinus with clival involvement, and 1 lesion was in the orbit (Table 2). The most common location of lesions in females was in the maxilla ($n = 5$). In males, the highest number of lesions was in the maxilla and mandible ($n = 3$ each). Of the 5 mandibular lesions, a multifocal mandibular involvement was seen in 1 patient, while the remaining 4 were solitary lesions, 2 of which were in the midline and 2 were peripherally located.

Nine of the 20 lesions had infiltrated into the surrounding bone and/or soft tissue. The orbital lesion extended into the fronto-ethmoid sinuses and into the nasal cavity. Parotid gland infiltration was present in 1 patient with GCG in the temporal bone. Intracranial extension was seen with 1 orbital, 2 sphenoidal, and 2 temporal bone GCGs, with extradural ($n = 1$), dural ($n = 4$), and cavernous sinus ($n = 2$) infiltration; brain parenchymal infiltration was not observed in any of these.

Imaging Features

Plain Radiography. Among the 9 patients who had plain radiographs obtained, the lesions were expansile, lytic, and well-circumscribed. There was no matrix mineralization in 8 of these 9 lesions; 1 patient had a sclerotic lesion with a ground-glass matrix.

CT Features of GCGs. On CT, 6 lesions had predominantly soft-tissue attenuation, 8 had fluid attenuation, 5 had mixed solid-cystic components, and 1 was sclerotic. Expansion and bony remodeling of the involved bone was observed in 15 lesions. Multiple loculations with thin septa were present in 10 lesions. Septal thickening with calcification was seen in 3 lesions. Tooth resorption was seen in 6 lesions involving the maxilla/mandible. There was heterogeneous enhancement of the soft-tissue component. None of the lesions had discrete foci of calcification. There was no encasement or hypertrophy of the adjacent blood vessels.

MR Imaging Features of GCGs. On MR imaging, the solid component was of intermediate-to-low signal intensity on T1WI and predominantly hypointense on T2WI, with interspersed heterogeneous areas of intermediate-to-high signal intensity. There was heterogeneous postcontrast enhancement of the solid areas. On visual assessment, there was an absence of diffusion restriction in the T2-hypointense areas. The ADC values in the areas of iso- to high signal intensity on the T2WI ranged between 8.45 and 1.06 × 10^{-3} mm^2/s. The fluid component in the GCGs was hypointense on T1WI and hyperintense on T2W1. Multiple fluid-fluid levels of differential signal intensity on T1WI and T2WI were present in 3 cases, indicative of hemorrhage.

Management and Follow-up

Preoperative embolization was performed in 1 patient. Six patients underwent complete surgical resection, and another 6 patients underwent partial or subtotal resection. Two patients underwent

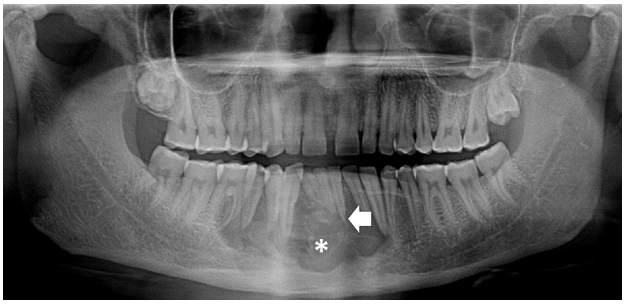

FIG 2. GCG of the mandible. Orthopantomogram shows an expansile, lytic central mandibular lesion with lobulated margins (*asterisk*). Note the resorption of the roots of the central incisors (*arrow*).

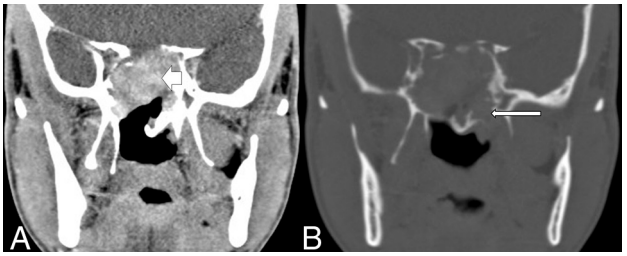

FIG 3. GCG of the sphenoid bone. *A*, Contrast-enhanced CT of the skull base shows a lobulated, enhancing mass in the sphenoid sinus (*short arrow*). *B*, On the bone window, the mass expands the sphenoid bone and there are multiple foci of a cortical breach (*long arrow*) Note the absence of matrix mineralization in the lesion.

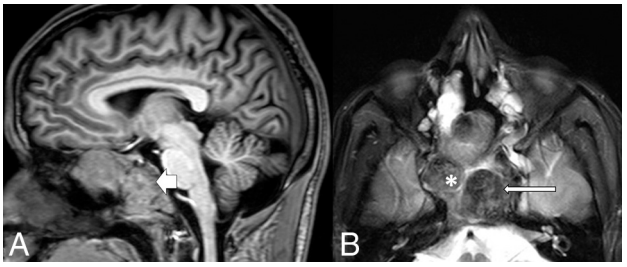

FIG 4. MR imaging features of GCG. *A*, Heterogeneous intermediate-to-high signal intensity (*short arrow*) on the T1-weighted sagittal image. *B*, Mixed intermediate-to-hyperintense (*white asterisk*) and hypointense (*long arrow*) solid components on T2-weighted axial image in the sphenoid bone and clival GCG.

postoperative radiation therapy. Postoperative follow-up imaging was available in 9 patients, with the follow-up period ranging from 4 months to 5 years. No intervention was performed in 7 patients who were lost to follow-up after diagnosis.

Of the 6 patients who underwent complete surgical resection of the lesions, postoperative follow-up imaging, which was available in 3 maxillary GCGs, showed disease recurrence in all 3 at an average interval of 39 months postsurgery. Clinicoradiologic progression occurred in 3 of the 5 patients who underwent subtotal or near-complete resection.

No features of malignant transformation were found in any of the lesions, either at primary imaging or in any of the follow-up imaging.

FIG 5. GCG of the orbit with secondary ABC changes appearing as a multiloculated lesion with multiple fluid-fluid levels (*arrow*) of differential signal intensity on T1-weighted (*A*) and T2-weighted (*B*) axial images.

DISCUSSION

GCGs are rare tumors of the head and neck, with a high propensity for recurrence. The rarity of the lesions, along with overlapping imaging features with certain benign as well as malignant lesions, make the preoperative diagnosis of GCGs challenging.

This study presents the observations of craniofacial GCGs in the single largest case series of imaging findings reported in the literature thus far. No age- or sex-specific predilection was observed in any site of involvement. We did not find any association of the lesions with trauma, pregnancy, or a previous malignancy.

On imaging, craniofacial GCGs have a variable appearance. On radiographs, the lesions are commonly solitary, expansile, and lytic (Fig 2). On CT, the lesions are commonly heterogeneous and multiloculated, with remodeling of the involved bone. Interrupted segments of focal cortical breach occur frequently, and this is a reliable indicator of these lesions being locally aggressive (Fig 3*B*). A soft-tissue component, when present, shows heterogeneous postcontrast enhancement (Fig 3*A*). Tooth resorption is a notable feature in GCGs of the mandible.

In the study by Nackos et al[5] in 7 patients, matrix mineralization was reported in all except 1 case, whereas this was an uncommon feature in our study.

On MR imaging in our study, the intralesional soft-tissue component was iso- to hypointense on T1WI sequences (Fig 4*A*). The lesions were heterogeneous on T2WI, with hypointense signal being the predominant finding (Fig 4*B*). This feature of hypointensity on T2WI is in keeping with the limited existing literature available on MR imaging features of GCGs and can be attributed to the presence of fibrous tissue and repetitive hemorrhage seen on histopathology.[5,14,15] Hemorrhage within the lesions appears as multiple fluid-fluid levels of differential signal intensity on T1WI and T2WI sequences (Fig 5). Layered SWI hypointensity can also be observed in multiloculated GCGs, indicating the hemorrhagic nature of the content (Fig 6). Three lesions with multiple fluid-fluid levels on MR imaging (1 in the orbit and 2 in the temporal bone) were reported as GCGs with secondary ABC changes on HPE.

The solid component of GCGs shows heterogeneous enhancement postcontrast (Fig 7*A*). Enhancement of the walls of the locules and septa is also a common feature (Fig 7*B*).

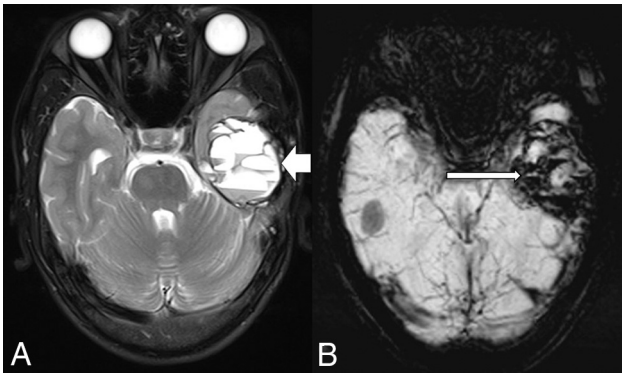

FIG 6. Multiloculated GCG of the left temporal bone with fluid-fluid levels (*short arrow*, *A*) on axial T2-weighted and layers of hypointense signal (*long arrow*, *B*) on a susceptibility-weighted imaging.

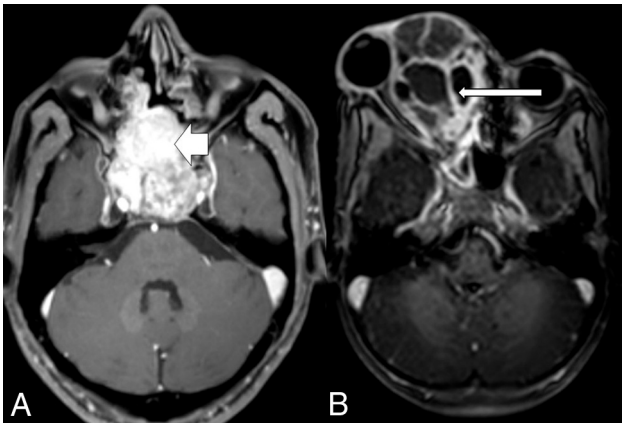

FIG 7. Patterns of enhancement in GCG (on postgadolinium TIWI). *A*, Solid, sphenoidal GCG shows heterogeneous enhancement (*short arrow*). *B*, Multiloculated right-orbital GCG with enhancing walls (*long arrow*).

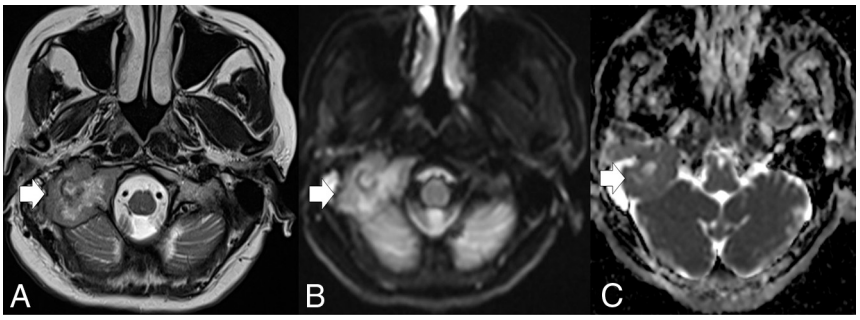

FIG 8. GCG of the right petrous bone. The lesion (*arrow*) is heterogeneous with peripheral, intermediate-signal-intensity soft tissue and central cystic area on (*A*) T2-weighted. DWI (*B*) and ADC map (*C*) of the lesion.

Features of GCG on DWI and ADC maps and on SWI have not been described in literature so far. Rao et al[16] found that an ADC value of 1.3 had the highest sensitivity and specificity in differentiating benign (high ADC) from malignant (low ADC) bone tumors. In the study by Nouh et al,[17] the mean ADC value of $\leq 1.1 \times 10^{-3}$ mm^2/s had a sensitivity of 86.1% for malignant bone lesions. DWI and ADC sequences available for 4 patients in our study did not show any diffusion restriction in the T2WI hypointense solid areas. Furthermore, the ADC values in the intermediate-to-high signal intensity areas were $>1.0 \times 10^{-3}$ mm^2/s (Fig 8). However, Ashikyan et al[18] found that GCTs also have a mean ADC of 1.1×10^{-3} mm^2. A larger sample size is required to arrive at a reliable conclusion on the ADC values of GCGs.

In our study, we observed that 12 patients had a combination of >1 aggressive feature. Additionally, 4 lesions demonstrated focal loss of a fat plane as a solitary aggressive feature. Thus, 80% ($n = 16/20$) were locally aggressive.

Recurrence or progression of residual tumor or both were observed in 6 of the 8 patients in whom postoperative follow-up imaging was available. Although the data available are scant, they imply that these lesions are locally aggressive and have an extremely high rate of recurrence, irrespective of the type of operation performed (total-versus-partial excision).

Differential Diagnosis of Craniofacial GCGs

Differentials for lytic, expansile lesions in the craniofacial and skull base bones include aneurysmal bone cyst, brown tumor of hyperparathyroidism, fibrous dysplasia, giant-cell tumors, giant-cell granulomas, and the whole gamut of odontogenic and nonodontogenic jaw lesions.[5,14,19-21]

ABCs are expansile, lytic lesions that are uncommon in the craniofacial bones. They are multiloculated with multiple fluid-fluid levels. Primary ABCs do not have a soft-tissue component. Secondary ABCs can occur with GCGs.[15] Failure to obtain adequate representative biopsy samples from different areas in a GCG can lead to sampling error and under-reporting of secondary ABC changes within the lesions.

A ground-glass matrix and bony remodeling are classic features of fibrous dysplasias; however, a hypointense soft-tissue component on T2WI is not.

Unilocular, cystic central GCGs could be indistinguishable from other cystic jaw and maxillary lesions on imaging, such as dentigerous cysts, odontogenic keratocysts, radicular cysts, and so forth. Cortical breach, however, is not seen in these lesions and they can also be readily differentiated from GCGs on histopathology.

Brown tumors of hyperparathyroidism and GCGs have a similar imaging and pathologic appearance.[3-5,14] While we conducted the present study, 1 patient with a lytic mandibular lesion on imaging and histopathologic features showing osteoclastic granulomas was found to have an elevated serum parathyroid hormone and a functioning parathyroid adenoma. This case was diagnosed as a brown tumor and excluded from the study.

The soft-tissue component in ameloblastoma is usually hyperintense on T2WI. Also in maxillary and mandibular carcinomas, the soft tissue is T2 hyperintense, along with extensive bony destruction and peritumoral fat stranding.

The soft-tissue component in both GCGs and GCTs is of intermediate-to-low signal intensity on T2WI. However, GCTs in the head and neck are extremely uncommon.[5,15,22] GCTs also have a potential to metastasize to other organs such as the lungs, a finding we did not observe with GCGs in our study. Given the considerable overlap in the imaging findings of GCGs and GCTs, it is imperative for the radiologist to be aware of these 2 entities and include both in the differential diagnosis of craniofacial lesions with a hypointense solid component on T2WI.

Limitations

Due to the rarity of craniofacial GCGs, only a limited sample size could be obtained for analysis. Because our study was retrospective in nature, imaging modalities, protocols, and MR imaging sequences were not uniform across all patients.

CONCLUSIONS

GCGs are rare, slow-growing, often painless tumor mimics of osseous lesions of the head and neck. As opposed to findings in the existing literature, no sex predilection or any association with trauma or pregnancy was noted in our study. Key imaging features of GCGs include solitary, expansile, lytic lesions with focal areas of cortical breach, and associated bony remodeling, often with mixed cystic and solid components. The solid component, when present, is hypointense on T2WI and enhances on postcontrast imaging but does not show diffusion restriction. Multiple fluid-fluid levels, when present, are indicative of secondary ABC changes within GCGs. Owing to a high rate of postoperative recurrence, it is imperative to assess, on imaging, all GCGs for aggressive features like tooth resorption, the presence of an extraosseous soft-tissue component, and the loss of plane with the surrounding structures.

ACKNOWLEDGMENT

We are grateful to Dr Pippa Deodhar, Scientist (grade IV), Principal's Office, Christian Medical College, Vellore, for helping us in revising this manuscript.

Disclosure forms provided by the authors are available with the full text and PDF of this article at www.ajnr.org.

REFERENCES

1. Jaffe HL. **Giant-cell reparative granuloma, traumatic bone cyst, and fibrous (fibro-osseous) dysplasia of the jawbones.** *Oral Surg Oral Med Oral Pathol* 1953;6:159–75 CrossRef Medline
2. Ackerman LV, Spjut HJ. **Giant cell reaction**. In: Firminger H, ed. *Atlas of Tumor Pathology: Tumors of Bone and Cartilage, fascicle 5, series 2.* Washington, DC: American Registry of Pathology 1962;293–314
3. Barnes L, Eveson JW, Reichart P, et al eds. *Pathology and Genetics of Head and Neck Tumours*. World Health Organization/International Agency for Research on Cancer; 2005
4. El-Naggar AK, Chan JK, Grandis JR, et al eds. *WHO Classification of Head and Neck Tumours*. Vol 9. 4th ed. World Health Organization/International Agency for Research on Cancer; 2017
5. Nackos JS, Wiggins RH, Harnsberger HR. **CT and MR imaging of giant cell granuloma of the craniofacial bones.** *AJNR Am J Neuroradiol* 2006;27:1651–53 Medline
6. Fechner RE, Fitz-Hugh GS, Pope TL. **Extraordinary growth of giant cell reparative granuloma during pregnancy.** *Arch Otolaryngol Chic Otolaryngol* 1984;110:116–19 CrossRef Medline
7. Nielsen GP, Rosenberg AE. *Diagnostic pathology: Bone*. Elsevier Health Sciences; 2021
8. Fletcher C. *Diagnostic Histopathology of Tumors*. 2 Volume Set. 5th ed. Elsevier; 2019
9. Oliveira AM, Perez-Atayde AR, Inwards CY, et al. **USP6 and CDH11 oncogenes identify the neoplastic cell in primary aneurysmal bone cysts and are absent in so-called secondary aneurysmal bone cysts.** *Am J Pathol* 2004;165:1773–80 CrossRef Medline
10. Presneau N, Baumhoer D, Behjati S, et al. **Diagnostic value of H3F3A mutations in giant cell tumour of bone compared to osteoclast-rich mimics.** *J Pathol Clin Res* 2015;1:113–23 CrossRef Medline
11. Scotto di Carlo F, Divisato G, Iacoangeli M, et al. **The identification of H3F3A mutation in giant cell tumour of the clivus and the histological diagnostic algorithm of other clival lesions permit the differential diagnosis in this location.** *BMC Cancer* 2018;18:358 CrossRef Medline
12. Nagar SR, Bansal S, Jashnani K, et al. **A comparative analysis of p63 expression in giant cell tumour (GCT), central giant cell granuloma (CGCG) and peripheral giant cell granuloma (PGCG).** *Head and Neck Pathol* 2020;14:733–41 CrossRef Medline
13. Ung F, Li KK, Keith DA, et al **Giant cell reparative granuloma of the temporal bone: case report and review of the literature.** *Otolaryngol Head Neck Surg* 1998;118:525–29 CrossRef Medline
14. Regezi JA. **Odontogenic cysts, odontogenic tumors, fibro-osseous, and giant cell lesions of the jaws.** *Mod Pathol* 2002;15:331–41 CrossRef Medline
15. Murphey MD, Nomikos GC, Flemming DJ, et al. **From the archives of AFIP: imaging of giant cell tumor and giant cell reparative granuloma of bone—radiologic-pathologic correlation.** *Radiographics* 2001;21:1283–309 CrossRef Medline
16. Rao A, Sharma C, Parampalli R. **Role of diffusion-weighted MRI in differentiating benign from malignant bone tumors.** *BJR Open* 2019;1:20180048 CrossRef Medline
17. Nouh MR, Doweidar A, Khalil AM. **Apparent diffusion coefficient (ADC): a potential in vivo biological surrogate of the incidentally discovered bone lesions at 3T MRI.** *Eur J Radiol Open* 2021;8:100386 CrossRef Medline
18. Ashikyan O, Chalian M, Moore D, et al. **Evaluation of giant cell tumors by diffusion weighted imaging-fractional ADC analysis.** *Skeletal Radiol* 2019;48:1765–73 CrossRef Medline
19. Shrestha S, Zhang J, Yan J, et al. **Radiological features of central giant cell granuloma: comparative study of 7 cases and literature review.** *Dentomaxillofac Radiol* 2021;50:20200429 CrossRef Medline
20. Jamil OA, Lechpammer M, Prasad S, et al. **Giant cell reparative granuloma of the sphenoid: case report and review of the literature.** *Surg Neurol Int* 2012;3:140 CrossRef Medline
21. Aralasmak A, Aygun N, Westra WH, et al. **Giant cell reparative granuloma of the sphenoid bone.** *AJNR Am J Neuroradiol* 2006;27:1675–77 Medline
22. Borges BB, Fornazieri MA, Correia de Araújo Bezerra AP, et al. **Giant cell bone lesions in the craniofacial region: a diagnostic and therapeutic challenge.** *Int Forum Allergy Rhinol* 2012;2:501–06 CrossRef Medline